SMC-TR-98-38

AEROSPACE REPORT NO.
TR-98(8555)-16

Volume Tolerance Characteristics of a Nickel-Hydrogen Cell

2 July 1998

Prepared by

L. H. THALLER, M. V. QUINZIO, and G. A. TO
Electronics Technology Center
Technology Operations

Prepared for

SPACE AND MISSILE SYSTEMS CENTER
AIR FORCE MATERIEL COMMAND
2430 E. El Segundo Boulevard
Los Angeles Air Force Base, CA 90245

Engineering and Technology Group

THE AEROSPACE CORPORATION
El Segundo, California

This report was submitted by The Aerospace Corporation, El Segundo, CA 90245-4691, under Contract No. F04701-93-C-0094 with the Space and Missile Systems Center, 2430 E. El Segundo Blvd., Los Angeles Air Force Base, CA 90245. It was reviewed and approved for The Aerospace Corporation by R. P. Frueholz Principal Director, Electronics Technology Center. P. Bissegger was the project officer for the Mission-Oriented Investigation and Experimentation (MOIE) program.

This report has been reviewed by the Public Affairs Office (PAS) and is releasable to the National Technical Information Service (NTIS). At NTIS, it will be available to the general public, including foreign nationals.

This technical report has been reviewed and is approved for publication. Publication of this report does not constitute Air Force approval of the report's findings or conclusions. It is published only for the exchange and stimulation of ideas.

Peter Bissegger
SMC/AXES

REPORT DOCUMENTATION PAGE

Form Approved
OMB No. 0704-0188

1. AGENCY USE ONLY (*Leave blank*)	2. REPORT DATE	3. REPORT TYPE AND DATES COVERED
	2 July 1998	

4. TITLE AND SUBTITLE

Volume Tolerance Characteristics of a Nickel-Hydrogen Cell

5. FUNDING NUMBERS

F04701-93-C-0094

6. AUTHOR(S)

L. H. Thaller, M. V. Quinzio, and G. A. To

7. PERFORMING ORGANIZATION NAME(S) AND ADDRESS(ES)

The Aerospace Corporation
Technology Operations
El Segundo, CA 90245-4691

8. PERFORMING ORGANIZATION REPORT NUMBER

TR-98(8555)-16

9. SPONSORING/MONITORING AGENCY NAME(S) AND ADDRESS(ES)

Space and Missile Systems Center
Air Force Materiel Command
2430 E. El Segundo Boulevard
Los Angeles Air Force Base, CA 90245

10. SPONSORING/MONITORING AGENCY REPORT NUMBER

SMC-TR-98-38

11. SUPPLEMENTARY NOTES

12a. DISTRIBUTION/AVAILABILITY STATEMENT

Approved for public release; distribution unlimited

12b. DISTRIBUTION CODE

13. ABSTRACT (*Maximum 200 words*)

The volume tolerance characteristics of a nickel-hydrogen cell were evaluated by altering the volume of electrolyte within the cell's components. This was done by evaporating increments of water from a cell and evaluating the cell's performance following each removal. The cell selected for this investigation was one that was sensitive to electrolyte volume reductions due to having only one layer of zircar separator. Two complete charge/discharge cycles were carried out following each water removal step. The discharge was programmed such that the cell was discharged at the C, C/2, and C/4 rates during the 100% depth-of-discharge. The discharge cycle was completed at the C/4 discharge rate to a 1.0-V cutoff voltage. Static modeling of this particular cell design permitted estimates to be made of the electrolyte content of the separator, the negative electrode, and the positive electrode following each increment of water removal. As expected, the internal impedance of the cell increased as the separator dried out, but there was no reduction in usable capacity at the C/2 rate after 57 ml of water had been removed from the cell. This represented a 26.7% reduction in the electrolyte volume. At this point, the static model estimated that only 15% of the pores within the separators were filled with electrolyte. These estimates of electrolyte content of the separator can be translated into estimates of cell performance following different amounts of electrode swelling and plaque corrosion that would result in equal amounts of electrolyte loss from the separator. During normal life cycle testing or mission applications, all three of these factors take place at the same time.

14. SUBJECT TERMS	15. NUMBER OF PAGES
Nickel-hydrogen, Volume tolerance, Cell dryout, destructive physical analysis	11
	16. PRICE CODE

17. SECURITY CLASSIFICATION OF REPORT	18. SECURITY CLASSIFICATION OF THIS PAGE	19. SECURITY CLASSIFICATION OF ABSTRACT	20. LIMITATION OF ABSTRACT
UNCLASSIFIED	UNCLASSIFIED	UNCLASSIFIED	

Acknowledgment

The cell used for this study was provided to us on loan by Eagle-Picher Industries. The contents of this report have been review by them and permission has been granted to publish these results.

Contents

Figures

Table

1. Background

Earlier studies addressing rates of performance degradation,[1,2] static modeling,[3] and electrolyte management considerations[4] for nickel-hydrogen cells have pointed out the problems that can be caused by separator dryout. Due to the smaller pore size characteristics of the nickel electrode relative to the separator,[5] capillary forces cause the separators to give up some of their electrolyte to the expanding nickel electrodes. The reactions associated with the electrochemical corrosion of the nickel plaque material[1] also result in a net loss of electrolyte volume. By modeling the effects of expansion of the positive plates as cycling progresses, and the corrosion of the porous nickel substrate material on the electrolyte content of the separator, it can be shown that there is a progressive loss of the amount and concentration of electrolyte that is contained within the separator.[3] Cells that have undergone extensive life cycle testing display reduced performance in terms of usable capacity and operating voltage during discharge.[6,7] Examination of the cell components following extended life cycle testing always reveals expanded and corroded positive plates.[2,8,9] Based on the destructive physical analysis (DPA) results carried out on cells that have been cycled extensively, it is not immediately obvious how to partition the performance degradation experienced during life cycle testing between effects caused by dryout of the separator and effects caused by swelling and corrosion damage to the positive electrodes.

Reductions in electrolyte content of the separator result in smaller amounts of electrolyte being available to carry the ionic current between the anodes and cathodes in the plate pack of the cell. This results in an increase in the internal resistance of the cell and can possibly result in what is called a diffusion-limiting current. A diffusion-limiting current is reached when there is an insufficient flow of ions to support the current being withdrawn from the cell. At this point, there is a rapid drop in the cell's operating voltage and current output. Electrode swelling reduces the usability of the active material due to the reduction in accessibility of electrons to the active material located within the pore structure of the nickel electrode. Electrode swelling also results in an increase in the internal resistance of the cell by drawing some of the electrolyte out of the separator and into the more wettable expanded pore structure of the nickel electrode. Plaque corrosion also results in a decrease in the usability of the active material in the porous structure of the nickel electrode. Plaque corrosion is caused by the oxidizing conditions present at the nickel electrodes during the recharge process. Some of the nickel material of the sinter and the screen located in the middle of the electrode is corroded to form nickel hydroxide. During this corrosion reaction, water from the electrolyte is partially consumed as per Eq. (1).

$$Ni + 2H_2O = Ni(OH)_2 + H_2 \quad (1)$$

There are two consequences of plaque corrosion. First, the corrosion product is a form of the active material but does not contain the cobalt additive of the material when it is impregnated into the electrode during its manufacture. Pure nickel hydroxide is less conductive than cobaltated material and also has a slightly higher charging voltage. Second, the corrosion of the junctures where the tiny nickel-carbonyl particles are sintered together are slowly destroyed. This reduces the mechanical

integrity of the conductive paths for the electrons to gain access to the active material. The increase in the average distance an electron must travel between the highly conductive nickel structure and the less conductive active material results in a increase in internal cell resistance. The resistance increase results in an earlier arrival to the low-voltage cutoff during discharge.

In an attempt to partition the effects of electrode expansion and separator dryout, it was proposed to carry out an experiment whereby the volume of electrolyte within a cell would be varied without appreciable corrosion or expansion of the nickel electrode.

2. Experimental

2.1 General

The experimental program could have been carried out in two ways. In the first, several cells of the same design could have been obtained that were filled with different amounts of electrolyte. This approach would have had several possible drawbacks. One drawback would have been the expense of obtaining 5 or 10 cells filled to our specifications. More importantly, it would have been difficult to be certain that each portion of the cell's multi-electrode plate pack would receive the same amount of electrolyte in cases where conditions of severe dryout were to be established. A second approach, and the one that was selected, was to obtain a cell that, by design, contained a small amount of electrolyte relative to the total wettable pore structure of the cell. The cell chosen contained one layer of zircar separator rather than the two layers used in the majority of cell designs. Alterations to the electrolyte volume would be accomplished by removing increments of water via evaporation. Following each increment of water removal, the cell would be evaluated for operating voltage and usable capacity by discharging the cell to 100% depth-of-discharge (DOD). Water removals would continue to the point where significant performance degradation was experienced by the cell. At this point, the cell would be opened, the separators and nickel electrodes would be analyzed for KOH content, and the nickel electrodes would be examined for possible increases in their thickness.

2.2 Experimental Procedure

A rabbit-eared, dual-stack, 100 A-h nickel-hydrogen cell was acquired for the test. A tube was welded onto the fill tube at the top of the dome. A valve and a 0-1000 PSIA pressure transducer were then attached to the tube. The cell was submerged in a constant-temperature bath and held at 10°C for all the electrical testing. For each electrical cycle, the cell was charged at a C/10 rate for 14 h (16 h for the first three charges), then stepped through a series of discharge rates (C/2 for 600 s, C/4 for 300 s, C for 300 s). This sequence was repeated four times. A final C/2 rate was then applied for 600 s, followed by a C/4 rate discharge to a 1.0-V low-voltage cutoff. The whole charge/discharge sequence was then repeated before the final discharge sequence of a C/10 discharge rate to a 1.0-V cutoff followed by a resistor let down to 0.0 V.

The cell was then removed from the bath and allowed to warm to room temperature. The weight of the cell was then obtained to an accuracy of 0.01g. The cell was then attached to a vacuum line (10^{-3} torr) fitted with a liquid-nitrogen vacuum trap. The cell was periodically removed from the line and weighed until the targeted amount of water was removed. The cell was ready for the next set of discharges. A total of seven water removal steps and performance evaluation sequences were conducted. At this point, the internal resistance of the cell had almost quadrupled in magnitude.

2.3 Post-Test DPA Procedure

After the final performance evaluation discharge had been completed, the cell case was opened by machining a cut around the cell on each side of the center weld ring. After the positive and the

negative terminals were cut off, the two pieces of the cell case were pulled away from the weld ring to expose the cell stack. The cell stack was disassembled, and each component was examined for defects such as blistering and popping. Both top and bottom stacks were disassembled. All positive plates were rinsed with deionized water to a neutral pH. Rinse water from plate pairs 2, 8, and 15 from both the upper and lower stacks were analyzed separately for total alkalinity by potentiometric titration to pH 4.5 with hydrochloric acid of known concentration. The same measurement was also made on the corresponding separators.

The rinsed positive plates were then air dried, and the plate thickness was measured on four different areas on each plate. The percentage increase in plate thickness (expansion) of each plate was calculated from the average of the four measurements and the original plate thickness of 35 mils.

3. Results

Some of the results will appear as calculations related to the percentage of the separator pores that are filled with electrolyte based on the static model developed for this cell. The amount of electrolyte added during its fabrication was supplied by the manufacturer. The static model used in this study[3] assumes that the separator will contain electrolyte that is in excess of the sum of the wettable pore volume of the thin hydrogen electrode and the much thicker nickel electrode. With each increment of water removal, the new volume and concentration of electrolyte were calculated. These numbers were inserted into the static model, and a revised estimate of the percentage of the separator's pores that were filled with electrolyte was calculated. Table 1 is a record of these calculations following each of the seven removal steps. For each step of water removal, equivalent amounts of expansion and corrosion of the positive plate were calculated that would have resulted in the same amount of electrolyte loss from the electrode/separator set. For completeness, this equivalent plate expansion is also expressed as a percentage of its original thickness. The electrodes in this cell were nominally 35 mils thick at the time the cell was built.

Other results appear as plots of cell performance and internal resistance as water was progressively removed from the cell. Figure 1 contains plots of the internal resistance of the cell as a function of the DOD and amount of water removed. The internal resistance was estimated by the change in cell voltage at the time there was a step change in cell discharge current. These values were relatively insensitive to the sequence and the DOD at which the values were calculated. The numbers along the ordinate are points where there was a step change in the discharge current. As the amount of electrolyte contained within the separator was reduced, the internal resistance of the cell increased. These values increased from about 1.0 milliohm prior to the removal of any water to as high as 4.0 milliohm at the point when it is estimated that only about 15% of the pores of the separator were filled with electrolyte. There are several apparent anomalous trends in this figure that merit comment. The resistance value of the case where 26.4 ml of water were removed is lower than the resistance value following the removal of 17.1 ml of water.

Table 1. Summary of Results of Water Removal Steps

Step	1	2	3	4	5	6	7	8
Water Removed (g)	0.0	9.6	17.1	26.4	33.9	43.7	50.0	57.3
Electrolyte in Cell (g)	279.6	269.6	262.1	252.1	244.6	235.86	229.6	223.7
KOH Concentration (%)	31.0	32.2	33.1	34.4	35.4	36.8	37.8	39.3
% of Separator Filled*	72	62	54	44	36	27	21	15
Equiv. % Expansion	0.0	4.0	7.4	11.9	15.5	20.1	23.9	26.9
Equiv. % Corrosion	0	4.6	7.2	13.1	15.9	19.9	22.8	26.5
Approx. Internal R (mOhm)	1.0	1.1	2.0	1.5	1.8	2.0	2.5	3.7

*Estimated from Aerospace Static Cell Model

This can be understood as due to the effects of not allowing enough time for the electrolyte to re-equilibrate within the cell following the removal of water. Drawing a vacuum on the cell as a means of removing water will most likely result in the preferential loss of water from the portions of the plate pack that are closest to the top of the cell. Following this, any maldistribution of electrolyte concentration will slowly be removed as the water from less concentrated portions of the electrolyte will move to regions of higher concentration under the influence of the gradients in the vapor pressure differences. The two high points on the line following 33.9 ml of water removal are examples of diffusion-limiting currents when 100 A were passed through the cell. (See also Figure 3). Since this condition was not seen following further removals of water, it is assumed that an insufficient amount of time was allowed for the re-equilibration of water between different parts of the plate pack following the water removal step.

Figure 2 shows the capacity charged into the cell during the charge steps and the capacity removed during the discharge steps to the 1.0-V cutoff at the C/4 rate. The cell maintained a usable capacity of about 113 A-h at the C/4 rate up to and including the last data point. The capacity to 0.0 V, including the resistor letdown following the second discharge sequence, was very close to the 140 A-h charged into the cell during the charge step. Figure 3 shows the composite discharge curves following different amounts of water removal from the cell. A point was reached where the cell was unable to maintain a voltage above 1.0 V during one or more portions of the discharge sequence. When a low-voltage limit was reached, the cell discharge programmer stepped the cell to the next preprogrammed discharge step. This resulted in an increase in the amount of capacity withdrawn from the cell during the final C/4 discharge step.

Each of the seven discharge sequences (only 4 shown here) showed a gradual decrease in the cell voltage as a consequence of the increase in internal resistance as indicated in Figure 1. The discharge curve following removal of 34 ml of water showed diffusion-limiting current problems at the last three applications of the C rate discharge.

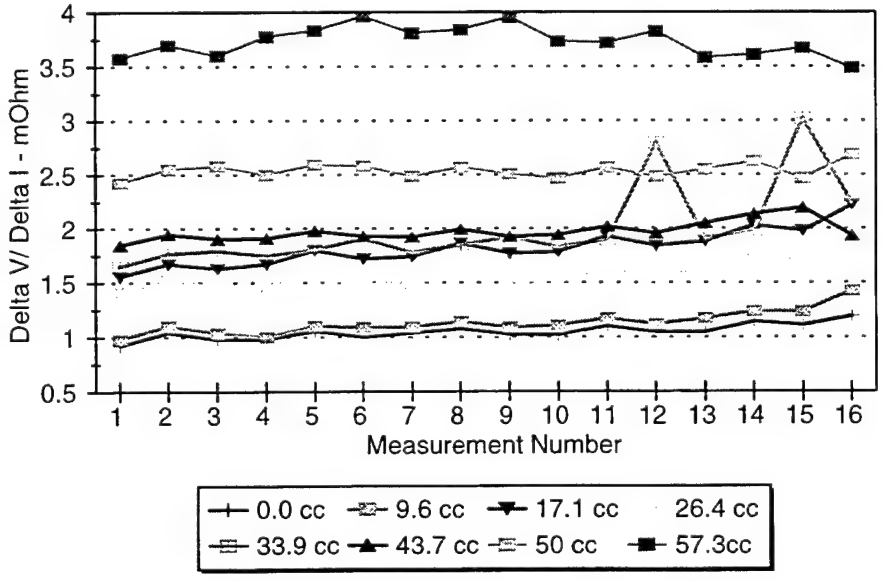

Figure 1. Internal cell resistance as water is removed.

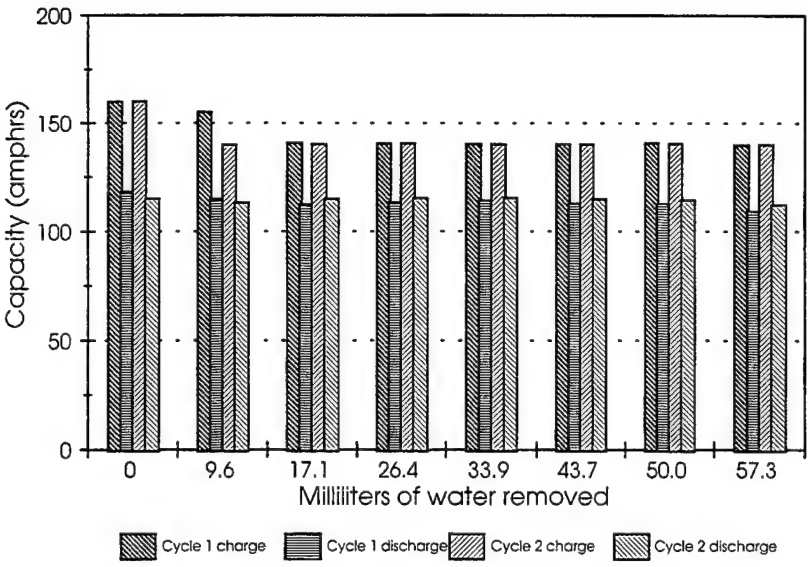

Figure 2. Ampere hours charged and ampere hours discharge to the 1.0 V.

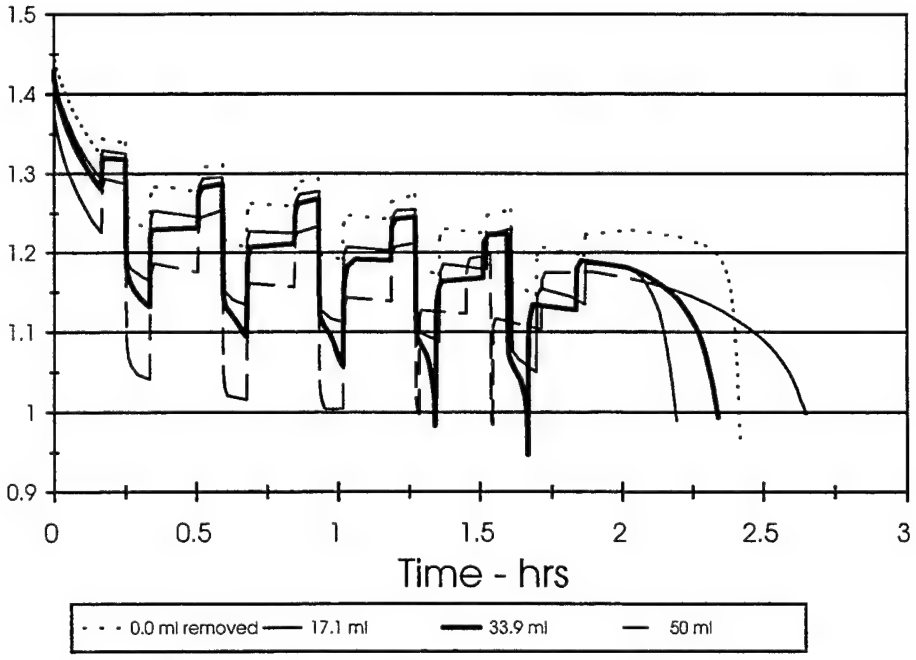

Figure 3. Discharge curves following water removal (1st cycle discharge).

Figure 4 shows the results of the KOH analyses carried out on six different electrode pairs and their corresponding separators. Three plate pairs were taken from both the top and bottom stacks of the cell (numbers 2, 8, and 15). The results show that the KOH contents of all plate pairs were very close no matter where they were located within the cell. This is evidence of a very uniform distribution of electrolyte across all 64 nickel electrodes. The results from the separators were also very uniform across the entire cell. The difference in the amount of KOH contained within the electrodes vs.

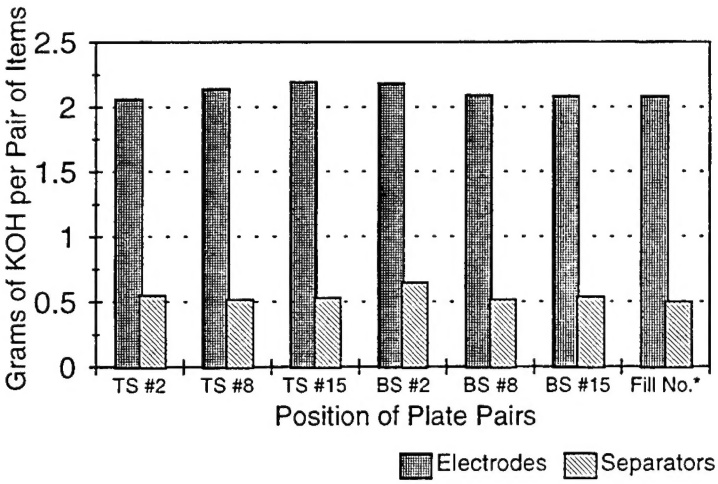

* Calculated using static model assuming no electrode expansion

Figure 4. KOH content of the nickel electrodes and separators.

that amount contained within the separators can be used to estimate the changes that occurred during the dryout steps within the cell. The static model contains information related to the porosities of all components within the cell. It further assumes that the separator will contain electrolyte that is in excess of the wettable pore volume of the nickel electrode and the hydrogen electrodes. With the densities of the different concentrations of KOH solutions and the electrolyte concentration following each water removal step, all the necessary information was available to allow calculation of the estimated distribution of electrolyte between the different cell components. Following the seventh removal step and the completion of the chemical analyses, the amounts estimated by the model can be evaluated for accuracy. The set of bars on the far right of Figure 4 is the estimate using the model. They agree very closely with the results of the chemical analyses. These calculation assumed zero expansion of the nickel electrodes. The average expansion was found to be 3.3%.

4. Conclusions

A flight-quality, nickel-hydrogen cell was modified so that increments of water could be evaporated as a technique to reduce the electrolyte volume available to the cell components. The impact of these water removal steps on the performance of the cell was evaluated by completely discharging the cell at several discharge rates. These discharges permitted the internal resistance of the cell to be estimated as a function of the DOD and the amount of water that was removed from the cell. The static model for this cell design was used to estimate the distribution of electrolyte between the different components within the cell. Following the last water removal and performance evaluation step, the cell was opened, and the components were analyzed for KOH content. This permitted the estimated distributions from the static model to be compared to the actual distributions from the results of the DPA analyses.

The cell performed very well as the volume of electrolyte was reduced. The internal resistance did increase, but at the lower discharge rate of C/4, the cell was still able to deliver the same capacity to the 1.0-V cutoff as when no water had been removed from the cell. The excellent agreement between the electrolyte distribution as estimated by our static cell model and the results of the chemical analyses validates the assumptions and numbers that are used in the calculation procedures used by the model.

References

1. Thaller, L.H., "Status of Degradation Rates and Mechanisms in Nickel-Hydrogen Cells," *Proc. of the 33rd IECEC*, To Be Published, Colorado Springs, CO, Aug. 2–8, 1998.

2. Lim, H. S. and Verzwyvelt, S. A., "Electrochemical Behavior of Heavily Cycled Nickel Electrodes in Nickel-Hydrogen Cells Containing Electrolytes of Various KOH Concentrations," *Proc. of the 16th International Power Sources Symposium*, pp. 341–355, Bournemouth, UK, Sept. 1988.

3. Thaller, L. H., "Volume-Based Static Model for Nickel-Hydrogen Cells," *Proc. of the 32nd IECEC* **1**, pp. 192–197, Honolulu, HA, July 27–Aug. 1, 1997.

4. Thaller, L. H. and Zimmerman, A. H., "Electrolyte Management Considerations In Modern Nickel-Hydrogen and Nickel-Cadmium Cell and Battery Designs," *J. Power Sources* **63**, (1996) 53–61.

5. Abbey, K. M. and Britton, D. L., "Pore Size Engineering Applied to the Design of Separators for Nickel-Hydrogen Cells and Batteries", *Proc. of the 18th IECEC* **4**, pp1552–1560, Orlando FL, Aug. 21–26, 1983.

6. Moore, B. A., Brown, H. M., and Miller, T. B., "International Space Station Nickel-Hydrogen Cell Testing at NAVSURFWARCENDIV Crane," *Proc. of the 32nd IECEC* **1**, pp. 174–179, Honolulu, HA, July 27–Aug. 1, 1997.

7. Moore, B. A., Brown, H. M., and Hill, C. A., "Air Force Nickel-Hydrogen Testing at NAVSURFWARCENDIV Crane," *Proc. of the 32nd IECEC* **1**, pp. 186–191, Honolulu, HA, July 27–Aug. 1, 1997.

8. Wheeler, J. R., "High Specific Energy Density, High Capacity Nickel-Hydrogen Cell Design," *Proc. of the 28th IECEC* **1**, pp. 89–94, Atlanta, GA, Aug. 8–13, 1993.

9. Lim, H. S. and Verzwyvelt, S. A., "Electrochemical Behavior of Heavily Cycled Nickel Electrodes in Nickel-Hydrogen Cells Containing Electrolytes of Various KOH Concentrations," *Proc. of the 16th International Power Sources Symposium*, pp. 341–355, Bournemouth, UK, Sept. 1988.

TECHNOLOGY OPERATIONS

The Aerospace Corporation functions as an "architect-engineer" for national security programs, specializing in advanced military space systems. The Corporation's Technology Operations supports the effective and timely development and operation of national security systems through scientific research and the application of advanced technology. Vital to the success of the Corporation is the technical staff's wide-ranging expertise and its ability to stay abreast of new technological developments and program support issues associated with rapidly evolving space systems. Contributing capabilities are provided by these individual Technology Centers:

Electronics Technology Center: Microelectronics, VLSI reliability, failure analysis, solid-state device physics, compound semiconductors, radiation effects, infrared and CCD detector devices, Micro-Electro-Mechanical Systems (MEMS), and data storage and display technologies; lasers and electro-optics, solid state laser design, micro-optics, optical communications, and fiber optic sensors; atomic frequency standards, applied laser spectroscopy, laser chemistry, atmospheric propagation and beam control, LIDAR/LADAR remote sensing; solar cell and array testing and evaluation, battery electrochemistry, battery testing and evaluation.

Mechanics and Materials Technology Center: Evaluation and characterization of new materials: metals, alloys, ceramics, polymers and composites; development and analysis of advanced materials processing and deposition techniques; nondestructive evaluation, component failure analysis and reliability; fracture mechanics and stress corrosion; analysis and evaluation of materials at cryogenic and elevated temperatures; launch vehicle fluid mechanics, heat transfer and flight dynamics; aerothermodynamics; chemical and electric propulsion; environmental chemistry; combustion processes; spacecraft structural mechanics, space environment effects on materials, hardening and vulnerability assessment; contamination, thermal and structural control; lubrication and surface phenomena; microengineering technology and microinstrument development.

Space and Environment Technology Center: Magnetospheric, auroral and cosmic ray physics, wave-particle interactions, magnetospheric plasma waves; atmospheric and ionospheric physics, density and composition of the upper atmosphere, remote sensing, hyperspectral imagery; solar physics, infrared astronomy, infrared signature analysis; effects of solar activity, magnetic storms and nuclear explosions on the earth's atmosphere, ionosphere and magnetosphere; effects of electromagnetic and particulate radiations on space systems; component testing, space instrumentation; environmental monitoring, trace detection; atmospheric chemical reactions, atmospheric optics, light scattering, state-specific chemical reactions and radiative signatures of missile plumes, and sensor out-of-field-of-view rejection.